^{89}Zr-DFO-AMG102 Immuno-PET to Determine Local Hepatocyte Growth Factor Protein Levels in Tumors for Enhanced Patient Selection

Eric W. Price[1], Kathryn E. Carnazza[1], Sean D. Carlin[1], Andrew Cho[1], Kimberly J. Edwards[1], Kuntal K. Sevak[1], Jonathan M. Glaser[1], Elisa de Stanchina[2], Yelena Y. Janjigian*[3], and Jason S. Lewis*[1,4]

[1]Department of Radiology, Memorial Sloan Kettering Cancer Center, New York, New York; [2]Antitumor Assessment Core Facility, Molecular Pharmacology Program, Memorial Sloan Kettering Cancer Center, New York, New York; [3]Gastrointestinal Oncology Service, Memorial Sloan Kettering Cancer Center, New York, New York; and [4]Program in Molecular Pharmacology, Memorial Sloan Kettering Cancer Center, New York, New York

The hepatocyte growth factor (HGF) binding antibody rilotumumab (AMG102) was modified for use as a ^{89}Zr-based immuno-PET imaging agent to noninvasively determine the local levels of HGF protein in tumors. Because recent clinical trials of HGF-targeting therapies have been largely unsuccessful in several different cancers (e.g., gastric, brain, lung), we have synthesized and validated ^{89}Zr-DFO-AMG102 as a companion diagnostic for improved identification and selection of patients having high local levels of HGF in tumors. To date, patient selection has not been performed using the local levels of HGF protein in tumors. **Methods:** The chelator *p*-SCN-Bn-DFO was conjugated to AMG102, radiolabeling with ^{89}Zr was performed in high radiochemical yields and purity (>99%), and binding affinity of the modified antibody was confirmed using an enzyme-linked immunosorbent assay (ELISA)–type binding assay. PET imaging, biodistribution, autoradiography and immunohistochemistry, and ex vivo HGF ELISA experiments were performed on murine xenografts of U87MG (HGF-positive, MET-positive) and MKN45 (HGF-negative, MET-positive) and 4 patient-derived xenografts (MET-positive, HGF unknown). **Results:** Tumor uptake of ^{89}Zr-DFO-AMG102 at 120 h after injection in U87MG xenografts (HGF-positive) was high (36.8 ± 7.8 percentage injected dose per gram [%ID/g]), whereas uptake in MKN45 xenografts (HGF-negative) was 5.0 ± 1.3 %ID/g and a control of nonspecific human IgG ^{89}Zr-DFO-IgG in U87MG tumors was 11.5 ± 3.3 %ID/g, demonstrating selective uptake in HGF-positive tumors. Similar experiments performed in 4 different gastric cancer patient-derived xenograft models showed low uptake of ^{89}Zr-DFO-AMG102 (~4–7 %ID/g), which corresponded with low HGF levels in these tumors (ex vivo ELISA). Autoradiography, immunohistochemical staining, and HGF ELISA assays confirmed that elevated levels of HGF protein were present only in U87MG tumors and that ^{89}Zr-DFO-AMG102 uptake was closely correlated with HGF protein levels in tumors. **Conclusion:** The new immuno-PET imaging agent ^{89}Zr-DFO-AMG102 was successfully synthesized, radiolabeled, and validated in vitro and in vivo to selectively accumulate in tumors with high local levels of HGF protein. These results suggest that ^{89}Zr-DFO-AMG102 would be a valuable companion diagnostic tool for the noninvasive selection of patients with elevated local concentrations of HGF in tumors for planning any HGF-targeted therapy, with the potential to improve clinical outcomes.

Key Words: AMG102; rilotumumab; hepatocyte growth factor; HGF; scatter factor; PET; MET; patient-derived xenograft

J Nucl Med 2017; 58:1386–1394
DOI: 10.2967/jnumed.116.187310

Hepatocyte growth factor (HGF), also called scatter factor, is a heterodimer protein that is normally synthesized by mesenchymal cells, including cancers such as sarcomas and high-grade gliomas (*1–7*). The sole receptor for the HGF ligand, MET (c-MET, mesenchymal-epithelial transition factor), is a transmembrane tyrosine kinase that is normally expressed in epithelial cells (*1*). Activation of MET by HGF binding results in deleterious effects in many cancers, and deregulation of MET activity is commonly responsible for tumorigenic properties and invasiveness (*6*). The increased invasive growth observed in tumors when MET is activated (e.g., by HGF binding or constitutive activation) is a result of pleiotropic biologic responses, including increased cell scattering, migration, invasion, and proliferation (*8*). Cancers that overexpress the MET receptor can be activated in a paracrine fashion by HGF produced from healthy mesenchymal cells in adjacent tissue, or by HGF made by mesenchymal cells within the bulk tumor or tumor cells, which results in a destructive autocrine loop for MET activation (*9*). For example, gliomas that function with these autocrine HGF loops contain higher concentrations of HGF and are more tumorigenic (*9*). Aggressiveness and invasiveness in MET-positive tumors can be experimentally enhanced by activation of MET by addition of HGF, and alternatively can be abolished by addition of HGF-specific inhibitors (*10–12*).

An understanding of the HGF/MET system reveals it as an obvious target for therapeutic pharmacologic intervention, and tyrosine kinase inhibitors as well as monoclonal antibodies have been developed to this end (Fig. 1) (*13*). A difficulty encountered in this field of study is identifying cancer cell lines—and more critically, patients—that possess autocrine HGF/MET loops and therefore high local HGF concentrations in tumors. The administration of HGF-neutralizing antibodies (including AMG102) to U118 and U87MG glioblastoma xenografts in mice (possessing

Received Nov. 16, 2016; revision accepted Feb. 15, 2017.
For correspondence or reprints contact: Jason S. Lewis, Department of Radiology, 1275 York Ave., Memorial Sloan Kettering Cancer Center, New York, NY 10065.
E-mail: lewisj2@mskcc.org
*Contributed equally to this work.
Published online Mar. 9, 2017.

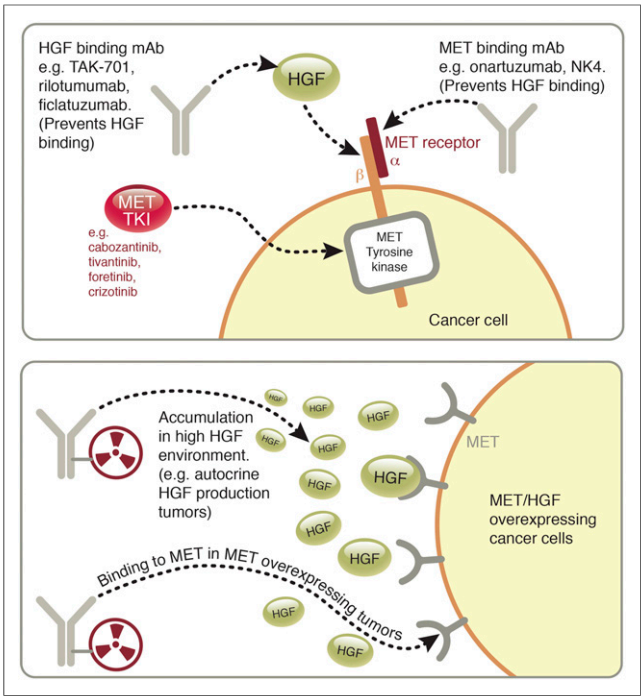

FIGURE 1. Graphic of MET/HGF system illustrating therapeutic approaches currently used to target it (top), including HGF-binding/neutralizing antibodies, MET-binding antagonists, and MET tyrosine kinase inhibitors, and depiction of antibodies tagged with radioactive metal (^{89}Zr) for use in immuno-PET of HGF/MET^{+} cancers (bottom).

autocrine HGF/MET loops) has resulted in reduced tumor growth when compared with an IgG control (*14,15*). Of 11 human gastric cancer cell lines (carcinomas) tested in a prior study, only SNU-484 was found to have HGF/MET autocrine loops (despite several of the tested cells lines expressing HGF messenger RNA [mRNA]) (*16*). In mouse models of gastric cancer, HGF/MET autocrine production was found only in MKN45 tumors and was found to promote metastasis (*17*). Although this study suggested that MKN45 gastric cancer cells possess HGF/MET autocrine loops, our assays have found no HGF expression in the MKN45 cells in our possession in vitro or in vivo (vide infra) (*17*). These examples show the difficulty in finding appropriate cancer models for this system but also demonstrate the ability of HGF-targeting therapies to exhibit the highest levels of efficacy in tumors that possess HGF/MET autocrine activation loops and high local levels of HGF. The importance of high local levels of HGF suggests that these subpopulations of tumors would be ideal candidates for targeted therapies of HGF/MET, and patients possessing high local levels of HGF in tumors would be ideal candidates for HGF-targeted treatments.

A large number of cancers have been reported to express HGF or MET clinically, and only a small percentage of patients within each cancer type has been reported to express HGF/MET autocrine loops (e.g., lung adenocarcinoma (*18*), muscle rhabdomyosarcoma (*19*), breast carcinoma (*20*), bone osteosarcoma (*21*), brain glioma (*9,22*)). Most human primary glioma and brain cancer cell lines have been found to produce their own HGF (*9,23*). The confounding factor in all of these studies is the lack of correlation between serum HGF levels and local HGF protein levels in tumor tissue. This suggests that there is a pressing need for a noninvasive method to directly measure local HGF protein levels in tumors before administration of HGF- or MET-targeted therapeutic drugs.

The Amgen Inc. antibody AMG102 is a fully human monoclonal antibody (IgG_2) that binds to and neutralizes HGF, thus preventing its binding to MET and therefore providing therapeutic effects. AMG102 has been tested in clinical trials for several different cancers, all with limited success to date. Despite a phase II trial of AMG102 in gastric cancer showing improved overall survival and progression-free survival, a recent phase III clinical trial of AMG102 in gastric cancer was terminated early (*24*). Because subjects have been evaluated by different methods in various studies—such as serum levels of HGF protein, local levels of MET protein in tumors (overexpression), and gene amplification (not always accompanied by transcriptional upregulation and overexpression of protein products)—finding appropriate autocrine HGF/MET cancer types and corresponding models is challenging (*25*). To our knowledge, patient selection for clinical trials of HGF-targeted drugs has not been attempted by measuring HGF levels directly in tumors, and although increased circulating HGF may be a prognostic factor in many cancers, it may be the wrong parameter to evaluate when investigating HGF-targeting therapies (*25*). No tools currently exist to noninvasively determine the levels of HGF present in the local tumor environment. Biopsies to measure HGF levels are not routinely performed, and because of the large heterogeneity within single tumors and even between different tumors/metastasis in a single patient, biopsy measurements are not accurate and therefore PET imaging would provide a superior whole-body picture of the HGF status of every lesion. To this end, we have developed a ^{89}Zr-based radioimmunoconjugate from the fully human antibody AMG102 to determine the local levels of HGF in tumors by PET imaging. Previous work toward molecular imaging of HGF is limited to an antibody fragment (Nanobody), which has been radiolabeled with ^{89}Zr and used to image HGF in U87MG glioblastoma xenografts with some success (*26*).

Retrospective Analysis of Clinical Patient Data

An evaluation of publicly available patient data on HGF mRNA expression and phosphoMET protein levels was performed to highlight relevant cancers for HGF-targeted drugs, because clinical trials of HGF-targeted drugs have been relatively unsuccessful to date (Fig. 2). Microarray-mRNA data suggest that lung adenocarcinoma (sample size, 32), glioblastoma multiforme (sample size, 473), and kidney renal clear cell carcinoma (sample size, 72) have statistically significantly higher levels of HGF mRNA than the other displayed cancer types, suggesting these cancers as clinically relevant subjects for future investigations of HGF-targeting drugs (Fig. 2A). More relevant for this study, protein levels of phosphoMET (activated MET, typically via HGF binding) in gastric cancer show a significant trend between phosphoMET quartile levels and survival. When activated by HGF binding, the MET receptor (tyrosine kinase) becomes phosphorylated to phosphoMET, suggesting a correlation between high levels of phosphoMET and HGF. Decreased survival times are observed between patients with higher phosphoMET protein levels (Q1 median survival, 609 days) compared with lower levels (Q4 median survival, 881 days) (Fig. 2B). This analysis of clinical data highlights the critical role of HGF and activated phosphoMET in tumor aggression and survival times and supports the hypothesis that local HGF protein levels should be

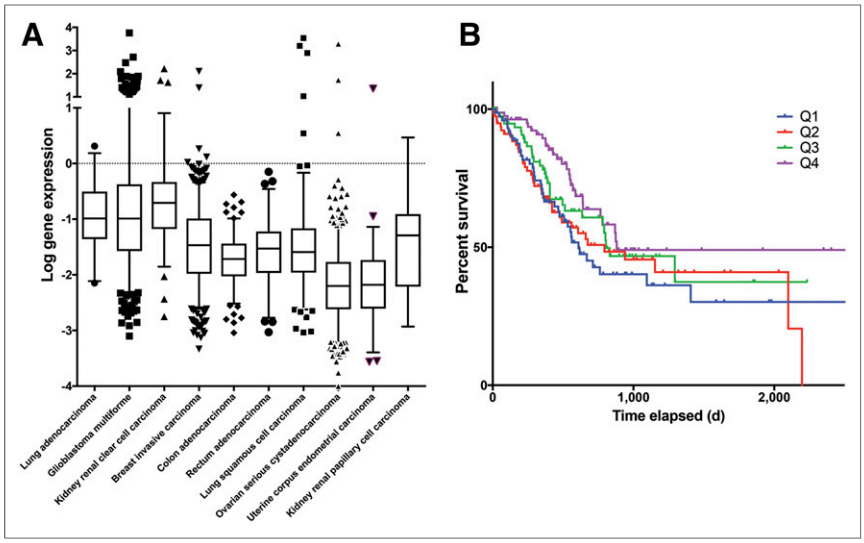

FIGURE 2. Evaluation of clinical patient data. (A) HGF mRNA levels in patients from micro-mRNA chip array data, showing a statistically significantly higher level of HGF mRNA expression (unadjusted $P < 0.00001$–0.00005, significant by 1-sided and 2-sided t tests, no correction for multiple comparisons) in lung adenocarcinoma (sample size, 32), glioblastoma multiforme (sample size, 473), and kidney renal clear cell carcinoma (sample size, 72) when compared with other cancer types displayed (no data for gastric cancer were available). (B) Survival curve for patients relating to protein levels of phosphoMET (activated MET receptor, usually by HGF binding) in gastric cancer patients, showing significance at 5% α-level by log-rank test for trend between the 4 quartile groups in survival times (top quartile median survival, 609 d; bottom quartile median survival, 881 d; 357 subjects) of phosphoMET levels. Results shown and discussed here are in whole or part based on data generated by the TCGA Research Network: http://cancergenome.nih.gov/.

evaluated in patient tumors before the administration of HGF-targeted therapies.

MATERIALS AND METHODS

General Procedures

All experiments were performed under a Memorial Sloan Kettering Institutional Animal Care and Use Committee–approved protocol, the experiments followed institutional guidelines for the proper and humane use of animals in research, and human tissue samples were collected for the Antitumor Assessment Core Facility under an approved institutional review board protocol. ^{89}Zr was produced at Memorial Sloan Kettering Cancer Center using an EBCO TR19/9 variable-beam energy cyclotron (Ebco Industries Inc.) via the ^{89}Y(p,n)^{89}Zr reaction. ^{89}Zr was purified in accordance with previously reported methods to create ^{89}Zr with a specific activity of 195–497 MBq/μg (5.3–13.4 mCi/μg) (*27*).

Evaluation of Clinical Patient Data

Raw patient data were obtained from the TCGA Research Network and parsed using an in-house MATLAB script. A level 3 reversed-phase protein array data was used to stratify the stomach adenocarcinoma cohort into quartiles of protein expression levels, and the survival time of each individual was determined using Clinical Biotab data. Each quartile is represented in a Kaplan–Meier survival curve, and this analysis was performed for phosphorylated MET and overall MET protein expression. Level 3 Agilent G4502A gene expression microarray data were used to generate MET and HGF RNA expression box plots. The cancer types used in these plots were selected based on the availability of level 3 Agilent G4502A gene expression microarray data in the TCGA database. The survival curves and box plots were generated using GraphPad Prism for Mac OS X (version 6.0f; GraphPad Software). The results shown and discussed here are in whole or part based upon data generated by the TCGA Research Network (http://cancergenome.nih.gov/).

Antibody Modification

AMG102 (lot #067A32374, obtained from Amgen Inc.) and a nonspecific human IgG antibody (from human serum, Sigma Aldrich) were purified using PD10 size-exclusion columns (PD10, Sephadex G-25 M, PD10 column [GE Healthcare]; phosphate-buffered saline [PBS], pH 7.4, 3 times), followed by centrifugal filter units (Amicon ultra centrifuge filters, Ultracel-50: regenerated cellulose, Millipore Corp.) (PBS, pH 7.4) to remove additives. After purification, the antibody (PBS, pH 7.4) was kept in the fridge at 4°C as a stock solution (~5–10 mg/mL). Subsequently, aliquots of each antibody solution (3.0 mg antibody) were combined with PBS (up to 1,000 μL total, pH 7.4), the pH of the resulting solution was adjusted to 8.8–9.0 with 0.1 M Na2CO3 (~30 μL), and 5 equivalents of p-SCN-Bn-DFO (Macrocyclics, Inc.) were added in 10–15 μL dimethyl sulfoxide. The reactions were incubated at 37 °C for 1 h, followed by PD10 purification and centrifugal filtration (Amicon 50 kDa) to purify the resultant antibody conjugate. The final immunoconjugate stock solutions were stored in PBS (pH 7.4) at 4°C.

Matrix-Assisted Laser Desorption/Ionization Time-of-Flight, Mass Spectrometry/Mass Spectrometry (MALDI-TOF MS/MS) Analysis to Determine the Number of Chelates per Antibody

The number of benzylthiourea-linked desferrioxamine (DFO) chelates conjugated to AMG102 was determined using MALDI-TOF MS/MS (Alberta Proteomics and Mass Spectrometry Facility, University of Alberta, Canada). All experiments were performed in triplicate, and all samples were run along with standard samples of unmodified AMG102 (run on the same day). One microliter of each sample (1 mg/mL) was mixed with 1 μL of sinapic acid (10 mg/mL in 50% acetonitrile:water and 0.1% trifluoroacetic acid). One microliter of the sample/matrix solution was then spotted onto a stainless steel target plate and allowed to air dry. All mass spectra were obtained using a Bruker Ultraflex MALDI-TOF/TOF (Bruker Daltonic GmbH). Ions were analyzed in positive mode, and external calibration was performed using a standard protein mixture (bovine serum albumin). The mass signals (M+2/2) at half of the parent molecular weight of the antibody were taken from each chromatogram and averaged ($n = 3$), and the average unmodified AMG102 weight was subtracted from the modified antibody weight to determine the mass contribution from conjugated chelator. The mass difference was divided by the molecular weight of the attached bifunctional chelator (p-SCN-Bn-DFO), and the error in each triplicate set of measurements (unmodified AMG102 vs. modified AMG102) was propagated to the final value of the number of chelates per antibody. Full MALDI-TOF spectra are shown in Supplemental Figs. 1–6 (available at http://jnm.snmjournals.org).

Determination of Antibody Binding Affinity

The immunoreactivity of ^{89}Zr-DFO-AMG102 could not be determined from typically utilized specific radioactive cellular-binding assays

because of HGF not being cell bound. In place of typical cell-binding assays, Immulon 2HB high-binding 96-well plates were coated with human HGF (HGF Recombinant Human Protein; Life Technologies) by adding 100 μL of an HGF solution in PBS (0.2 μg/mL, 200 ng/mL) and mixing overnight at 4°C. HGF-coated plates were aspirated/rinsed 3 times with PBS/0.2% tween (PBST). HGF-coated plates were then blocked with 100 μL of 3% bovine serum albumin–PBS for 1 h at room temperature. Blocking solution was aspirated/rinsed 3 times with PBST. Samples of unmodified AMG102 and the immunoconjugate DFO-AMG102 (60 μg/mL) were added to the first wells (125 μL), and a serial dilution (1/5, 25 μL transferred from each well, leaving a total of 100 μL per well) was performed 11 times, yielding wells with concentrations from 60 – 1 x 10^{-6} μg/mL in 100 μL total volume in each well. A nonspecific human IgG isotype antibody was also used as a control for nonspecific binding. Antibody solutions were allowed to sit for 1 h at room temperature. Plates were washed 3 times with PBST, followed by adding 100 μL of rabbit anti–human horseradish peroxidase secondary antibody (1/130,000 dilution, from 2 mg/mL stock, ab6759 Abcam) and incubating for 1 h at room temperature. The plates were then aspirated/rinsed 3 times with PBST, followed by enzymatic reaction detections by addition of a 1:1 mixture of peroxidase substrate solution B and TMB peroxidase substrate (100 μL per well, KPL TMB microwell peroxidase substrate system) and incubating for 10 min at room temperature. Development was stopped by addition of H_2SO_4 (0.1 M, 100 μL per well). Plates were read at 450 nM on a Molecular Devices SpectraMax M5 plate reader. Data were plotted and analyzed in PRISM software to determine half maximal effective concentration values.

ELISA Assay for HGF Protein Levels in Spent Medium, Serum, and Tumor Homogenates

ELISA assay kits for detecting human HGF were obtained from Life Technologies (Novex, KAC2211). For cell medium, spent medium was harvested after 5 d of incubation, and medium was analyzed by the ELISA kits with concentrations of 1:1, 1:5, 1:10, and 1:100. HGF protein could be detected only in the 1:1 concentration of spent U87MG cell medium. For serum samples of U87MG, MKN45, and PDX tumor–bearing mice, blood was obtained either by retroorbital bleed or by terminal cardiac puncture (no heparin was added due to ELISA interference). Blood was allowed to sit on ice for 30 min and was then centrifuged at 600*g* for 15 min to separate blood cells and clotting factors. The straw-colored blood serum was decanted by pipet and was analyzed by an ELISA kit in concentrations of 1:1, 1:10, and 1:100. Tumor samples were homogenized by taking a solid piece of tumor and adding 250 μL of RIPA buffer, 2.5 μL of protease inhibitor cocktail (abcam), mechanically homogenizing, sonication, and then centrifugation to remove debris. Tumor homogenates were normalized for protein concentration using a BCA assay to 100 μg of protein per well.

Western Blot Analysis of Cell Lines for MET Expression

For immunoblot assays, cells were harvested and cell pellets were resuspended in RIPA buffer with protease and phosphatase inhibitor cocktails (Calbiochem) and sonicated. After protein quantification, lysates were run on 7% precast NuPAGE Tris-Acetate gels (Thermo-Fischer Scientific), transferred to Immobilon-P PVDF membrane (EMD Millipore), blocked in 7% non-fat milk (Carnation), incubated in primary antibody solution for 1 h at room temperature, washed, incubated in secondary antibody solution for 30 min at room temperature, washed, and exposed. Antibodies were used at the following concentrations in TBS-T to probe the blots: 1:5,000 MET (Anti-Met [c-Met] antibody [EP1454Y] ab51067; Abcam), 1:20,000 actin. Appropriate secondary antibodies were used at 1:5,000 for MET (rabbit anti–human horseradish peroxidase; Abcam) and 1:7,500 for actin. Chemiluminescence was used to visualize protein expression with ECL on film (Amersham ECL Prime; GE Healthcare).

Cell Culture

Flasks containing cells were stored in cell incubators maintained at 37°C and a 5% CO_2 concentration. Cell lines were harvested weekly using a formulation of 0.25% trypsin/0.53 mM EDTA in Hank's Buffered Salt Solution without calcium and magnesium, which was then neutralized with at least 200% the volume of trypsin with the appropriate medium containing fetal bovine serum.

The human ovarian cancer cell line SKOV3 (cultured in McCoy's 5A Medium, modified to contain 1.5 mM L-glutamine and 2,200 mg/L sodium bicarbonate), human glioblastoma cell line U87MG (cultured in Dulbecco's modified Eagle's medium, 2 mM L-glutamine, 1,500mg/L sodium bicarbonate), human gastric carcinoma cell line Kato III (cultured in Iscove's modified Dulbecco's medium [IMDM] containing 4 mM L-glutamine, 4,500 mg/L glucose, and 1,500 mg/L sodium bicarbonate), and human gastric cancer cell line NCI-N87 (cultured in RPMI-1640 medium modified to contain 2 mM L-glutamine, 10 mM HEPES, 1 mM sodium pyruvate, 4,500 mg/L glucose, and 1,500 mg/L sodium bicarbonate) were all grown with 100 units/mL penicillin G and 100 μg/mL streptomycin and 10% fetal bovine serum, and were purchased from American Type Culture Collection.

The human gastric cancer cell line MKN45 (cultured in RPMI-1640 medium modified to contain 2 mM L-glutamine, and 1,500 mg/L sodium bicarbonate) and human gastric carcinoma cell line GTL-16 (cultured in Dulbecco's modified Eagle's high glucose medium, 2 mM L-glutamine) were grown with 10% fetal bovine serum, 100 units/mL penicillin G, and 100 μg/mL streptomycin, and were obtained from Dr. Martin R. Weiser's laboratory at MSKCC.

^{89}Zr Radiolabeling of DFO-AMG102 and DFO-IgG

Aliquots of chelate-modified antibody (350 μg) were transferred to 2-mL microcentrifuge tubes and made up to approximately 0.5 mL with phosphate-buffered saline (pH 7.4, treated with chelex resin at 1.2 g/L chelex overnight before use; BioRad Laboratories). Aliquots of ^{89}Zr-oxalate were neutralized to about pH 7.0–7.4 using sodium carbonate (1 M) and subsequently mixed with the DFO-AMG102 and DFO-IgG samples (~74 MBq [~2.0 mCi]) and reacted for 60 min at 37°C. Radiochemical yields obtained were greater than 98% after 1 h by radio–instant thin-layer chromatography (iTLC) (ethylenediaminetetraacetic acid mobile phase, 50 mM, pH 5) using silica-gel impregnated glass microfiber paper strips (iTLC-SG; Varian) (analyzed by AR-2000; Bioscan Inc.). ^{89}Zr-labeled antibodies were then purified using size-exclusion chromatography (PD10), followed by centrifugal filtration (Amicon ultra 50k, with saline) to concentrate the final volume for formulation. The radiochemical purity of the final purified radiolabeled antibodies was confirmed to be greater than 99% by radio-iTLC before injection. The ^{89}Zr-DFO-AMG102 radioimmunoconjugate was assessed for stability in human blood serum (Sigma) for 7 d at 37°C (radio-iTLC).

MKN45 and U87MG Xenograft Mouse Models

Eight- to 10-wk-old athymic *nu/nu* female mice (NCRNU-M) were obtained from Charles River Laboratories. Animals were housed in ventilated cages, were given food and water ad libitum, and were allowed to acclimatize for approximately 1 wk before treatment. After several days, MKN45 and U87MG tumors were induced on the left shoulder by a subcutaneous injection of 8.0×10^6 cells in a 100-μL cell suspension of a 1:1 mixture of fresh medium/BD Matrigel (BD Biosciences). Experiments were performed approximately 2 wk after the injection of the cancer cells.

Patient-Derived Xenograft (PDX) Mouse Models

PDX models were established from tumor specimens collected under an approved institutional review board protocol and have been arbitrarily designated DF, DY, DC, and EK to ensure no patient information is shared. Briefly, tumors were minced, mixed with Matrigel, and implanted subcutaneously in 6- to 8-wk-old female NSG

mice (Jackson Laboratories). Once established, tumors were maintained and expanded by serial subcutaneous transplantation. All patient samples had gastric human epidermal growth factor receptor 2 (HER2)–positive tumors. DF and DY were from the same patient at different stages of disease. Tumor samples were evaluated by immunohistochemistry and graded for HER2 and MET expression, with DC, DF, DY, and EK all being graded 3+ for HER2 expression (high), and 3+, 1–2+, 2+, and 3+ for MET, respectively. HGF levels in these tumors were not evaluated before this study.

^{89}Zr-DFO-AMG102 PET Imaging

PET imaging was performed using a small-animal PET rodent scanner (Focus 120; Concord Microsystems). Mice were administered radiolabeled antibody (~30 μg, ~4.8–5.6 MBq [~130–150 μCi]) in 200 μL of sterile saline (0.9% NaCl) via intravenous tail injection. Approximately 5 min before PET image acquisition, mice were anesthetized via inhalation of a 2% isoflurane–oxygen gas mixture (Baxter Health Care) and placed on the scanner bed where anesthesia was maintained. PET images were acquired at 24, 48, 72, and 120 h, with PET data being recorded via static scans with a minimum of 15 million coincident events (~20–30 min). An energy window of 350–700 keV and a coincidence timing window of 6 ns were used. Data were sorted into 2-dimensional histograms by Fourier rebinning, and transverse images were reconstructed by filtered backprojection into a 128 × 128 × 63 (0.72 × 0.72 × 1.3 mm) matrix. The image data were normalized to correct for nonuniformity of response of the PET, dead-time count losses, positron branching ratio, and physical decay to the time of injection, but no attenuation, scatter, or partial-volume averaging correction was applied. The counting rates in the reconstructed images were converted to activity concentrations (percentage injected dose per gram of tissue [%ID/g]) by use of a system calibration factor derived from the imaging of a mouse-sized water-equivalent phantom containing ^{89}Zr. Images were analyzed using ASIPro VM software (Concorde Microsystems).

^{89}Zr-DFO-AMG102 and ^{89}Zr-DFO-IgG Biodistribution Studies

Mice bearing subcutaneous xenografts as described above were intravenously injected through the tail vein with either ^{89}Zr-DFO-AMG102 or ^{89}Zr-DFO-IgG (0.74–1.1 MBq [~20–30 μCi], ~5 μg, in 200–250 μL of sterile saline; tumor volume, ~100–150 mm^3). Mice were euthanized by CO_2 (g) asphyxiation at time points of 24, 48, 72, and 120 h (n = 5/time point). Organs collected after sacrifice included blood, tumor, heart, lungs, liver, spleen, pancreas, kidneys, large intestine, small intestine, muscle, bone (femur), and skin (ear). All organs were rinsed in water after removal and air-dried for 5 min. The organs from ^{89}Zr biodistribution experiments were placed in preweighed test tubes, weighed again to obtain tissue weights, and the amount of radioactivity present was determined using an Automated Wizard γ-Counter (Perkin-Elmer). The counts were background- and decay-corrected from the time of injection and then converted to %ID per gram of organ tissue (%ID/g). The radioactivity counts measured in each organ were converted to activity (μCi) using a calibration curve created from known standards of ^{89}Zr (serial dilution from ~0.1 MBq [~3 μCi] of ^{89}Zr). The gastric cancer PDX mice (DF, DY, DC, EK) imaged with ^{89}Zr-DFO-AMG102 were euthanized for biodistribution experiments immediately after their final imaging point (120 h).

Autoradiography and Histology

After PET imaging and excision of tumors, a subset of tumors was embedded in optimal-cutting-temperature mounting medium (OCT; Sakura Finetek) and frozen on dry ice. Series of 10-μm frozen sections were then cut. To determine radiotracer distribution, digital autoradiography was performed by placing tissue sections in a film cassette against a phosphor imaging plate (Fujifilm BAS-MS2325; Fuji Photo Film) for an appropriate exposure period at −20°C. Phosphor imaging plates were read at a pixel resolution of 25 μm with a Typhoon 7000 IP plate reader (GE Healthcare). After autoradiographic exposure, the same frozen sections were then used for immunohistochemical (IHC) staining and microscopy. IHC staining of HGF and perlecan was performed using antibodies LS-B4957 (1:50 dilution; Life Span Biosciences) and A7L6 (5 μg/mL; ThermoFisher), respectively, and secondary detection with species-appropriate secondary antibodies conjugated to Alexafluor-568 and Alexafluor-488, respectively. Sequential sections were stained with hematoxylin and eosin.

Whole mount images were acquired at 100× magnification using a BX60 microscope (Olympus America, Inc.) equipped with a motorized stage (Prior Scientific Instruments Ltd.) and DP80 camera (Olympus). Whole-tumor montage images were obtained by acquiring multiple fields at 40× magnification, followed by alignment using MicroSuite Biologic Suite (version 2.7; Olympus). IHC and autoradiographic images were registered using Adobe Photoshop (CS6) as previously described (*28*).

RESULTS

Bioconjugation, Radiolabeling, and In Vitro Characterization

To begin, AMG102 was incubated under slightly basic conditions (pH 9.0) with 5 equivalents of *p*-SCN-Bn-DFO and purified via size-exclusion chromatography (PD10) and spin filtration (Amicon Ultra 50 kDa). After purification, aliquots of AMG102 immunoconjugates were frozen and sent for analysis by matrix-assisted laser desorption/ionization time-of-flight mass spectrometry analysis. Mass spectrometry results indicated that these modifications yielded 1.0 ± 0.1 chelates per antibody (Supplemental Figs. 1–6; Supplemental Table 1). Determination of immunoreactivity (e.g., immunoreactive fraction) could not be performed by a standard immunoreactivity cell-binding assay (*29*), because the target antigen HGF is a circulating growth factor and not a cell surface–bound receptor. An enzyme-linked immunosorbent assay (ELISA)–based binding assay was therefore performed to compare binding affinity values of AMG102, DFO-AMG102, and a nonspecific human IgG, which confirmed little change in binding affinity (K_d = equilibrium dissociation constant between antibody and antigen, measure of binding affinity) for DFO-AMG102 (0.64 vs. 0.83 nM K_d, literature 0.22 nM (*3*)) (Fig. 3B). DFO-AMG102 was then radiolabeled with ^{89}Zr in phosphate-buffered saline (pH 7.4, treated with Chelex resin) for 60 min at 37°C. Radiochemical yields were evaluated using radio-iTLC, and a mobile phase of ethylenediaminetetraacetic acid (pH 5, 50 mM) was used to resolve free ^{89}Zr from antibody-bound radiometal, which confirmed greater than 98% crude radiochemical yields and greater than 99% radiochemical purity after PD10 purification (Fig. 3A). Before using the new radioimmunoconjugate ^{89}Zr-DFO-AMG102, appropriate cancer models were selected. Available gastric cancer cell lines were grown in culture, and the spent medium (5-d incubation time) was harvested and analyzed by ELISA for HGF content. It was determined that the only cell line producing detectable quantities of HGF was U87MG glioblastoma, which has been previously studied in the literature with HGF-targeting antibodies (Fig. 3D). Because the antibody AMG102 does not recognize or bind murine HGF, a suitable cell line was required for this initial study that possessed an autocrine HGF/MET loop and therefore would contain high local levels of HGF in tumor models (*6,8*), and so U87MG cells were selected. MET expression in U87MG (HGF-positive [HGF$^+$]) and MKN45 (HGF-negative [HGF$^-$]) cells was confirmed by Western blot analysis (Fig. 3C).

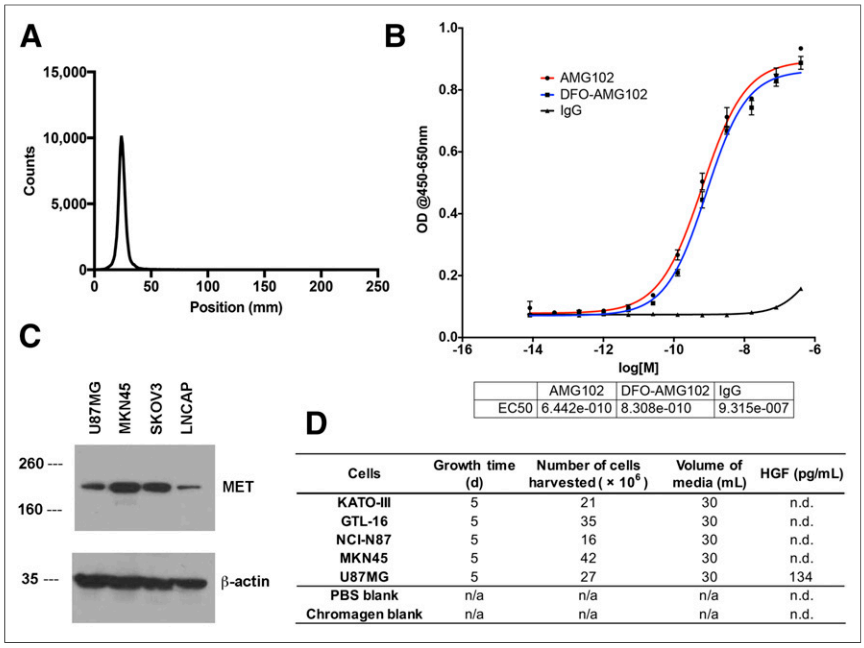

	AMG102	DFO-AMG102	IgG
EC50	6.442e-010	8.308e-010	9.315e-007

Cells	Growth time (d)	Number of cells harvested (× 10^6)	Volume of media (mL)	HGF (pg/mL)
KATO-III	5	21	30	n.d.
GTL-16	5	35	30	n.d.
NCI-N87	5	16	30	n.d.
MKN45	5	42	30	n.d.
U87MG	5	27	30	134
PBS blank	n/a	n/a	n/a	n.d.
Chromagen blank	n/a	n/a	n/a	n.d.

FIGURE 3. Results for radiolabeling, binding affinity, and cancer cell line selection. (A) ^{89}Zr-DFO-AMG102 radiochemical purity by radio-iTLC, showing > 99.5% radiochemical purity after purification by PD10 column (free ^{89}Zr elutes at ~100–125 mm). (B) Binding assay comparing modified DFO-AMG102 with unmodified AMG102. (C) Western blot results from MET/HGF-producing U87MG cells, MET-producing MKN45 cells, SKOV3 ovarian cancer cells for reference, and LNCAP cells as a low-MET-expressing reference. (D) Results from an ELISA assay for human HGF showing amount of HGF produced by select cell lines in spent medium.

^{89}Zr-DFO-AMG102 PET Imaging Studies in U87MG and MKN45 Murine Subcutaneous Xenografts

Female nude athymic mice were inoculated with subcutaneous xenografts (8×10^6 cells, left shoulder) of U87MG (HGF$^+$, MET$^-$ positive [MET$^+$], $n = 4$) or MKN45 (HGF$^-$, MET$^+$, $n = 4$, controls) tumors, and ^{89}Zr-DFO-AMG102 was administered via intravenous tail injection for serial PET imaging studies (~30 μg, ~4.8–5.6 MBq [~130–150 μCi], 200 μL of sterile saline). PET images were acquired at 24, 48, 72, and 120 h after injection, showing a steady increase in U87MG tumor uptake (~40 %ID/g at 120 h after injection) with a concomitant decrease in blood-pool/background activity during the 120-h imaging study (Fig. 4). Control images obtained in mice bearing MKN45 xenografts revealed high blood-pool and background activity at all time points, with tumor uptake remaining low at 5–10 %ID/g throughout the duration of the study (Fig. 4).

Biodistribution Studies of ^{89}Zr-DFO-AMG102

Radiolabeled and purified ^{89}Zr-DFO-AMG102 was injected via the tail vein into mice bearing subcutaneous U87MG (autocrine, HGF$^+$, MET$^+$, $n = 5$) or MKN45 (HGF$^-$, MET$^+$, $n = 10$, control) xenografts on the left shoulder (0.74–1.1 MBq [~20–30 μCi], ~5 μg, in 200–250 μL of sterile saline; tumor volume, ~100–150 mm^3). After time points of 24, 48, 72, and 120 h ($n =$ 5/time point), the mice were euthanized via CO_2 (g) asphyxiation followed by cervical dislocation, after which 14 organs including the tumors were removed, weighed, and assayed for radioactivity using an automated γ-counter. Control biodistributions were performed in U87MG tumor–bearing mice with both ^{89}Zr-DFO-IgG (nonspecific isotype human IgG) and a blocking group that was coinjected with cold AMG102 (100-fold, 500 μg). These controls were performed to confirm selective uptake of ^{89}Zr-DFO-AMG102 in HGF+ tumors beyond uptake from the enhanced permeability and retention (EPR) effect. Biodistribution data demonstrated substantial uptake of ^{89}Zr-DFO-AMG102 in HGF+ tumors (U87MG), reaching 36.8 ± 7.8 %ID/g at 120 h after injection (Supplemental Tables 2–5). This result compared favorably with 2 controls that showed low tumor uptake values of 5.0 ± 1.3 and 11.5 ± 3.3 % ID/g for HGF− tumors (MKN45) and ^{89}Zr-DFO-IgG in U87MG tumors, respectively. Organ ratios were calculated from ^{89}Zr-DFO-AMG102 biodistribution data and revealed tumor-to-blood (T/B), tumor-to-heart (T/H), and tumor-to-liver (T/L) ratios to be excellent in U87MG tumors when compared with MKN45 controls (T/B = 2.4 ± 0.6 vs. 0.4 ± 0.1, T/H = 7.5 ± 1.6 vs. 1.7 ± 0.5, T/L = 6.6 ± 1.5 vs. 1.0 ± 0.4, respectively, Supplemental Table 5).

^{89}Zr-DFO-AMG102 PET Imaging in PDXs

The radioimmunoconjugate ^{89}Zr-DFO-AMG102 was prepared and injected in mice bearing subcutaneous PDX tumors as described above, and serial PET imaging was performed at 24, 48, 72, and 120 h, with necropsy, tissue harvesting, and biodistribution analysis performed after 120-h

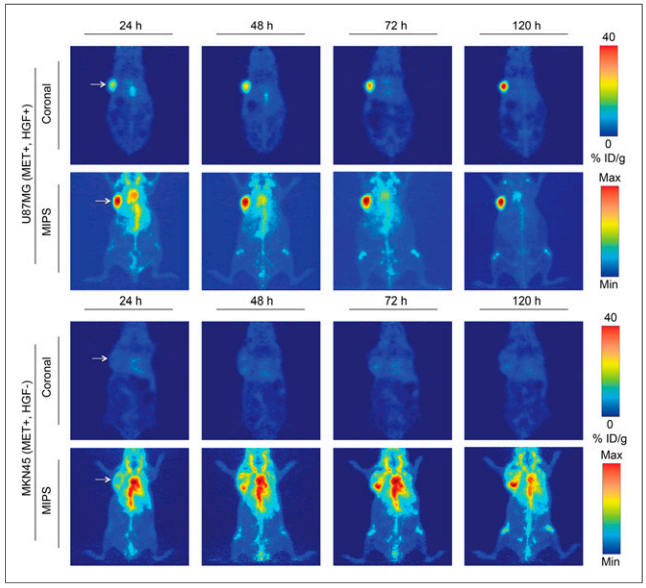

FIGURE 4. Serial PET imaging of ^{89}Zr-DFO-AMG102 in positive (U87MG HGF$^+$, MET$^+$) and negative (MKN45 HGF$^-$, MET$^+$) mouse xenografts (~30 μg, ~4.8–5.6 MBq [~130–150 μCi], 200 μL of sterile saline), showing selective and high uptake in tumors that possess high local HGF protein levels (U87MG, ~40 %ID/g) and low uptake in tumors with low HGF levels (MKN45, ~5–10 %ID/g, EPR uptake only). Max = maximum; Min = minimum.

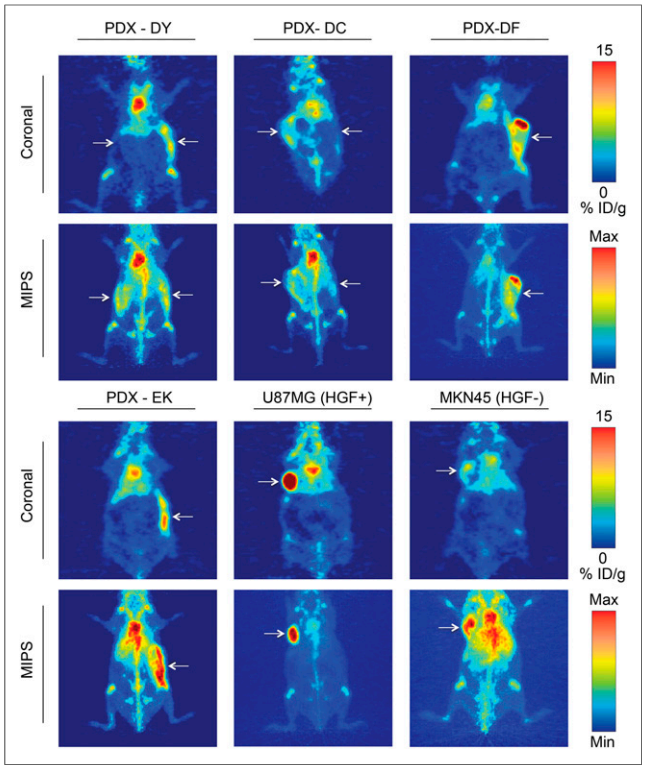

FIGURE 5. ^{89}Zr-DFO-AMG102 (~30 μg, ~4.8–5.6 MBq [~130–150 μCi], 200 μL of sterile saline) PET images 120 h after injection comparing uptake in different tumor types, showing high uptake in HGF$^+$ U87MG tumors (~40 %ID/g) and low uptake in HGF$^-$ MKN45 tumors (~5–10 %ID/g). Mice bearing gastric PDXs (DY, DC, DF, EK) with previously unknown levels of HGF show similarly low uptake to the HGF$^-$ MKN45 xenografts, noninvasively determining little or no HGF present. Tumors are highlighted with white arrows, and images with 2 arrows indicate bilateral xenografts (DY, DC); full serial PET images are in Supplemental Figures 8–9.

PET imaging. The PET images in Figure 5 are all 120 h after injection and are compared with U87MG (HGF+ control) and MKN45 (HGF− control) xenografts, with PDX tumor uptake ranging between 5 and 10 %ID/g.

^{89}Zr-DFO-AMG102 Biodistribution, Autoradiography, and Immunohistochemistry in PDXs

Biodistribution experiments were performed on the PDX-bearing mice shown in Figure 5, after 120-h PET imaging. The uptake of ^{89}Zr-DFO-AMG102 in PDX tumors was confirmed to be low (~4–7 %ID/g), which corroborates the PET imaging data displayed in Figure 5 that suggested low uptake of approximately 5–10 %ID/g (nonspecific EPR uptake) (Fig. 6B, data in Supplemental Table 6). To validate these results using additional quantitative methods, tumor and blood serum samples were obtained from mice bearing PDX and U87MG/MKN45 tumors and were analyzed using an ELISA kit for HGF. The ELISA results confirm that the only tumors that contained high levels of HGF were U87MG (3.31 ng/mg of protein), with MKN45 and PDX tumors containing HGF levels of only 0.02–0.26 ng/mg of protein, which aligns well with reported normal levels of HGF in human tissue of 0.22 ± 0.32 ng/mg of protein (Fig. 6C) (*17,30*). The HGF protein concentrations determined by ELISA aligned well with the observed tumor uptake values (%ID/g) of ^{89}Zr-DFO-AMG102 in tumors by PET imaging and biodistributions (Figs. 5 and 6C). These results in U87MG xenografts reveal that despite having high intratumoral HGF protein levels, no HGF could be detected in blood serum (Fig. 6C). This study provides further credence to the idea that local HGF protein levels in tumors must be assessed because serum levels may not accurately predict intratumoral levels.

During tissue harvesting and biodistribution analysis, tumor sections were taken and autoradiography and IHC were performed on the ^{89}Zr-DFO-AMG102–containing samples (Fig. 7). Autoradiography and IHC demonstrated uptake of ^{89}Zr-DFO-AMG102 largely in the stroma and areas of vasculature (basement membrane/extracellular matrix) of the MKN45 (HGF$^-$) tumors, which would

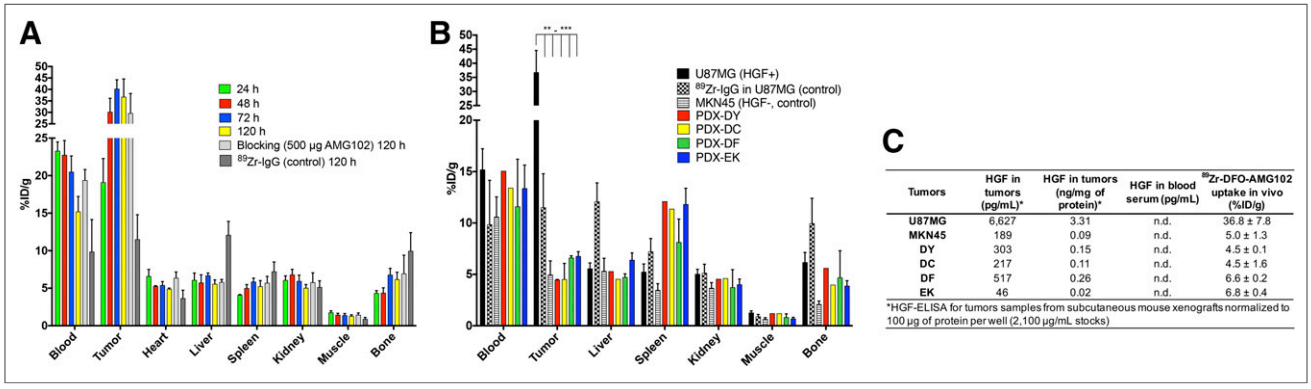

Tumors	HGF in tumors (pg/mL)*	HGF in tumors (ng/mg of protein)*	HGF in blood serum (pg/mL)	^{89}Zr-DFO-AMG102 uptake in vivo (%ID/g)
U87MG	6,627	3.31	n.d.	36.8 ± 7.8
MKN45	189	0.09	n.d.	5.0 ± 1.3
DY	303	0.15	n.d.	4.5 ± 0.1
DC	217	0.11	n.d.	4.5 ± 1.6
DF	517	0.26	n.d.	6.6 ± 0.2
EK	46	0.02	n.d.	6.8 ± 0.4

*HGF-ELISA for tumors samples from subcutaneous mouse xenografts normalized to 100 μg of protein per well (2,100 μg/mL stocks)

FIGURE 6. (A) Biodistribution data from ^{89}Zr-DFO-AMG102 in female nude mice bearing U87MG subcutaneous xenografts from 24 to 120 h after injection (~0.74–1.11 MBq [~20–30 μCi], ~5 μg), including controls of ^{89}Zr-IgG (nonspecific human IgG antibody) and blocking dose (500 μg, 100-fold cold AMG102 coinjected), showing substantial uptake in U87MG tumors with high local levels of HGF, low uptake of control ^{89}Zr-DFO-IgG (EPR effect), and no apparent blocking effect (see "Discussion" section). (B) Biodistribution data at 120 h after injection showing ^{89}Zr-DFO-AMG102 and ^{89}Zr-DFO-IgG (control) (~0.74–1.11 MBq [~20–30 μCi], ~5 μg) in U87MG (HGF$^+$, MET$^+$) and MKN45 (control, HGF$^-$, MET$^+$), and data from 4 different gastric PDXs at 120 h after injection showing low tracer uptake from ^{89}Zr-DFO-IgG control in U87MG and ^{89}Zr-DFO-AMG102 in MKN45, and similarly low uptake of ^{89}Zr-DFO-AMG102 in the 4 PDX models (HGF levels previously unknown). (C) Data from ELISA assay for human HGF (pg/mL), and normalized HGF levels (ng/mg of protein) showing HGF levels in tumor homogenates and blood serum samples of tumor-bearing mice and corresponding in vivo %ID/g uptake values of ^{89}Zr-DFO-AMG102. Statistical significance shown from Student unpaired *t* test using PRISM software, $^*P = \leq 0.05$, $^{**}P \leq 0.01$, $^{***}P = \leq 0.001$, with all tumor uptake comparisons to U87MG having statistical significance between $^{**}P$ and $^{***}P$.

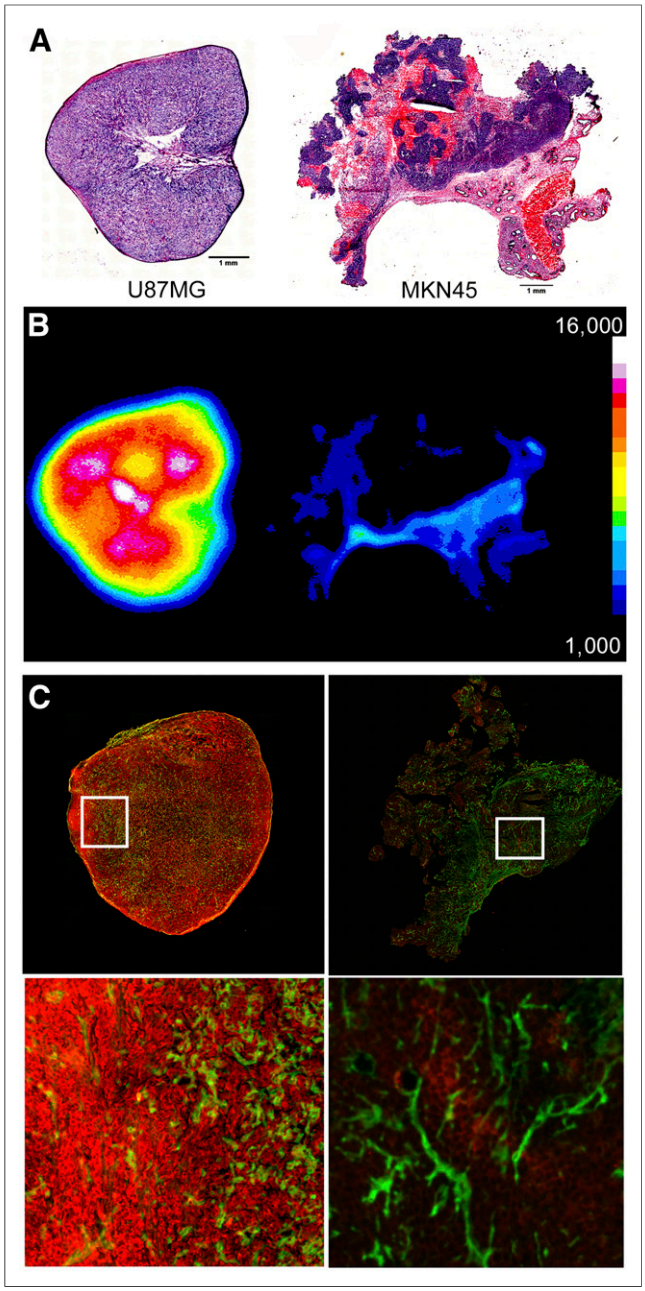

FIGURE 7. Sections of tumors obtained at time of necropsy after PET, showing hematoxylin and eosin staining (U87MG left, MKN45 right) (A), autoradiography for U87MG (left, high uptake) and MKN45 (right, low uptake) (B), and immunofluorescence staining shown in green for perlecan (extracellular matrix/stroma) and red for anti-HGF (U87MG left, MKN45 right) (C), confirming high concentrations of HGF protein only in U87MG tumors.

be consistent with nonspecific EPR uptake (Fig. 7). Of interest is the fact that HGF is a low-affinity binder to the glycoprotein heparin sulfate, which retains HGF in the stroma and limits diffusion out of the tumors (*31*). These tumor sections were additionally stained for perlecan (green, heparin sulfate glycoprotein in stroma) and human HGF (red), to see whether colocalization could be observed. No significant colocalization of ^{89}Zr-DFO-AMG102, HGF, and perlecan could be observed from this immunofluorescent staining (Fig. 7). High levels of HGF in U87MG tumor sections relative to MKN45 tumors was confirmed, which also mimics autoradiography results showing higher uptake of ^{89}Zr-DFO-AMG102 selectively in U87MG tumors. Similar autoradiography and immunofluorescence staining were performed on PDX tumor sections, which confirmed low uptake of ^{89}Zr-DFO-AMG102 and low levels of HGF (Supplemental Figs. 10–12).

DISCUSSION

PET imaging, biodistribution, immunohistochemistry, and autoradiography and ex vivo ELISA experiments with ^{89}Zr-DFO-AMG102 have demonstrated selective and high uptake in tumors that contain high levels of HGF protein. Uptake of ^{89}Zr-DFO-AMG102 was very low (background uptake, from the EPR effect) in tumors that did not contain high local concentrations of HGF (MKN45), whereas uptake was high in tumors that contained high local levels of HGF (U87MG). The blocking experiment that used an excess of nonradioactive AMG102 appears unsuccessful when looking at tissue-weight normalized uptake values (%ID/g, Fig. 6A). Supplemental Fig. 7A shows these same data as non-normalized uptake values (%ID), which suggests at least partial blocking of tumor uptake. This could be a result of the dramatic therapeutic effect observed from the blocking dose of AMG102 (500 μg), which resulted in a substantial decrease in tumor size (0.06 ± 0.03 g blocking vs. 0.21 ± 0.05 g nonblocking, $n = 5$, Supplemental Fig. 7B). Although the tissue-weight normalization (%ID/g) should account for this tumor size difference, such a dramatic difference in tumor size doesn't appear to be appropriately corrected for, possibly due to high levels of antigen (HGF) and the small injected dose of antibody (~5 μg) not saturating target binding (HGF) in either scenario. Further to this point, the biodistribution blocking data shown in Supplemental Fig. 7A as %ID reveal equivalent uptake in all organs except the tumor (statistically significantly lower uptake in blocked tumor). Not all targets can effectively be blocked with reasonable doses, and due to the high levels of HGF produced by U87MG tumors, the blocking dose of 500 μg may not have been sufficient. Problematically, this dose was sufficient for a dramatic therapeutic effect (Supplemental Fig. 7B), suggesting that blocking studies are not effective controls for this specific imaging agent. It has been previously shown in mice bearing xenografts of U87MG cells that AMG102 has a substantial therapeutic effect when compared with control groups (*15*), and these results were confirmed during this study (Supplemental Fig. 7B).

These nonstandard blocking results are not entirely convincing, but are also not of serious concern because a second control experiment was performed and successfully demonstrated selective uptake of ^{89}Zr-DFO-AMG102 in tumors with high HGF levels (U87MG, 36.8 ± 7.8 %ID/g, 120 h after injection) and low uptake in HGF$^-$ tumors (MKN45, 5.0 ± 1.3 %ID/g, 120 h after injection) by both PET imaging and biodistribution studies (HGF levels quantitatively confirmed by ELISA assay, Figs. 4 and 6B). A third control experiment was also successful and demonstrated lower uptake of a nonspecific isotype control antibody ^{89}Zr-DFO-IgG in HGF$^+$ U87MG tumor xenografts (11.5 ± 3.3 %ID/g, 120 h after injection) compared with ^{89}Zr-DFO-AMG102 (36.8 ± 7.8 %ID/g, 120 h after injection) via biodistribution of tumor-bearing mice (Fig. 6A).

To evaluate the ability of ^{89}Zr-DFO-AMG102 to noninvasively determine local HGF protein levels in tumors, 4 different PDXs were obtained that all had confirmed MET expression by immunohistochemistry, but had unknown levels of HGF. Only a small number of PDX-bearing mice were available, and some were bilateral xenografts that contained the same PDX tumor type on both

flanks. These PDX PET imaging results suggest the limited uptake of ^{89}Zr-DFO-AMG102 was largely a result of nonspecific EPR uptake (as with control experiments), and the range in uptake between 5 and 10 %ID/g is likely attributed to variations in vasculature and blood flow between these different PDX tumors (full serial-PET images, Supplemental Figs. 8 and 9). Because successful control experiments with ^{89}Zr-DFO-AMG102 have demonstrated it to be selective for HGF-positive tumors, these results provide a noninvasive measure of the levels of HGF protein in these PDX tumors. These results suggest that these specific PDX contain low levels of HGF protein and therefore would not be suitable candidates for administration of a therapeutic regiment of AMG102 or any other HGF-targeting drug, because they would not be likely to respond.

CONCLUSION

The HGF binding antibody AMG102 was successfully modified for use as a ^{89}Zr-based immuno-PET imaging agent to noninvasively determine local HGF protein levels in tumors. Uptake of ^{89}Zr-DFO-AMG102 at 120 h after injection in U87MG (HGF^+) xenografts (36.8 ± 7.8 %ID/g) was statistically significantly higher than in control tumors (MKN45, HGF−, 5.0 ± 1.3 %ID/g) and in ^{89}Zr-DFO-IgG nonspecific isotype control in U87MG (11.5 ± 3.3 %ID/g). Similar experiments performed in 4 different gastric cancer PDX models showed low uptake of ^{89}Zr-DFO-AMG102 (~4–7 %ID/g), which corresponded with low HGF levels in these tumors as determined by ELISA assay of tumor homogenates and serum samples. Taken together, these results craft a compelling story that the new immuno-PET imaging agent ^{89}Zr-DFO-AMG102 would be a valuable companion diagnostic tool for selection of patients who possess high local HGF protein levels in tumors, and would therefore be more likely to respond to any HGF-targeted therapy.

DISCLOSURE

Eric W. Price was supported by the Natural Sciences and Engineering Research Council (NSERC) (PDF, 2014-2016). The MSKCC Small-Animal Imaging Core Facility, supported in part by NIH Small-Animal Imaging Research Program (SAIRP) grant no. R24 CA83084 and NIH Center grant no. P30 CA08748, are gratefully acknowledged. The Radiochemistry and Molecular Imaging Probe Core is also supported in part by NIH center grant P30 CA08748. The Antitumor Assessment Core thanks Core grant P30 CA008748 and PDX support from U54 grant U54 OD020355. No other potential conflict of interest relevant to this article was reported.

ACKNOWLEDGMENTS

We acknowledge Dr. Kristen Cunanan (MSKCC, Epidemiology & Biostatistics) for assistance in reporting the statistical analysis of clinical patient data and Dr. Freddy Escorcia (MSKCC, Radiation Oncology) for thoughtful editing.

REFERENCES

1. Bottaro DP, Rubin J, Faletto D, et al. Identification of the hepatocyte growth factor receptor as the c-met proto-oncogene product. *Science.* 1991;251:802–804.
2. Cecchi F, Rabe DC, Bottaro DP. Targeting the HGF/Met signaling pathway in cancer therapy. *Expert Opin Ther Targets.* 2012;16:553–572.
3. Cecchi F, Rabe DC, Bottaro DP. The hepatocyte growth factor receptor: structure, function and pharmacological targeting in cancer. *Curr Signal Transduct Ther.* 2011;6:146–151.
4. Cecchi F, Rabe DC, Bottaro DP. Targeting the HGF/Met signalling pathway in cancer. *Eur J Cancer.* 2010;46:1260–1270.
5. Jiang WG, Martin TA, Parr C, Davies G, Matsumoto K, Nakamura T. Hepatocyte growth factor, its receptor, and their potential value in cancer therapies. *Crit Rev Oncol Hematol.* 2005;53:35–69.
6. Corso S, Comoglio PM, Giordano S. Cancer therapy: can the challenge be MET? *Trends Mol Med.* 2005;11:284–292.
7. Comoglio PM, Boccaccio C. Scatter factors and invasive growth. *Semin Cancer Biol.* 2001;11:153–165.
8. Giordano S. Rilotumumab, a mAb against human hepatocyte growth factor for the treatment of cancer. *Curr Opin Mol Ther.* 2009;11:448–455.
9. Koochekpour S, Jeffers M, Rulong S, et al. Met and hepatocyte growth factor/scatter factor expression in human gliomas. *Cancer Res.* 1997;57:5391–5398.
10. Michieli P, Basilico C, Pennacchietti S, et al. Mutant Met-mediated transformation is ligand-dependent and can be inhibited by HGF antagonists. *Oncogene.* 1999;18:5221–5231.
11. Rong S, Segal S, Anver M, Resau JH, Vande Woude GF. Invasiveness and metastasis of NIH 3T3 cells induced by Met-hepatocyte growth factor/scatter factor autocrine stimulation. *Proc Natl Acad Sci USA.* 1994;91:4731–4735.
12. Abounader R, Lal B, Luddy C, et al. In vivo targeting of SF/HGF and c-met expression via U1snRNA/ribozymes inhibits glioma growth and angiogenesis and promotes apoptosis. *FASEB J.* 2002;16:108–110.
13. Scagliotti GV, Novello S, von Pawel J. The emerging role of MET/HGF inhibitors in oncology. *Cancer Treat Rev.* 2013;39:793–801.
14. Cao B, Su Y, Oskarsson M, et al. Neutralizing monoclonal antibodies to hepatocyte growth factor/scatter factor (HGF/SF) display antitumor activity in animal models. *Proc Natl Acad Sci USA.* 2001;98:7443–7448.
15. Rex K, Lewis XZ, Gobalakrishnan S, et al. Evaluation of the antitumor effects of rilotumumab by PET imaging in a U-87 MG mouse xenograft model. *Nucl Med Biol.* 2013;40:458–463.
16. Park M, Park H, Kim W-H, Cho H, Lee J-H. Presence of autocrine hepatocyte growth factor-Met signaling and its role in proliferation and migration of SNU-484 gastric cancer cell line. *Exp Mol Med.* 2005;37:213–219.
17. Toiyama Y, Yasuda H, Saigusa S, et al. Co-expression of hepatocyte growth factor and c-Met predicts peritoneal dissemination established by autocrine hepatocyte growth factor/c-Met signaling in gastric cancer. *Int J Cancer.* 2012;130:2912–2921.
18. Siegfried JM, Weissfeld LA, Singh-Kaw P, Weyant RJ, Testa JR, Landreneau RJ. Association of immunoreactive hepatocyte growth factor with poor survival in resectable non-small cell lung cancer. *Cancer Res.* 1997;57:433–439.
19. Ferracini R, Olivero M, Di Renzo MF, et al. Retrogenic expression of the MET proto-oncogene correlates with the invasive phenotype of human rhabdomyosarcomas. *Oncogene.* 1996;12:1697–1705.
20. Tuck AB, Park M, Sterns EE, Boag A, Elliott BE. Coexpression of hepatocyte growth factor and receptor (Met) in human breast carcinoma. *Am J Pathol.* 1996;148:225–232.
21. Ferracini R, Di Renzo MF, Scotlandi K, et al. The Met/HGF receptor is overexpressed in human osteosarcomas and is activated by either a paracrine or an autocrine circuit. *Oncogene.* 1995;10:739–749.
22. Birchmeier C, Birchmeier W, Gherardi E, Vande Woude GF. Met, metastasis, motility and more. *Nat Rev Mol Cell Biol.* 2003;4:915–925.
23. Rosen EM, Laterra J, Joseph A, et al. Scatter factor expression and regulation in human glial tumors. *Int J Cancer.* 1996;67:248–255.
24. Cunningham D, Tebbutt NC, Davidenko I, et al. Phase III, randomized, double-blind, multicenter, placebo (P)-controlled trial of rilotumumab (R) plus epirubicin, cisplatin and capecitabine (ECX) as first-line therapy in patients (pts) with advanced MET-positive (pos) gastric or gastroesophageal junction (G/GEJ) cancer: RILOMET-1 study. *J Clin Oncol.* 2015;33(suppl May 2015):4000.
25. Zhang Y, Jain R, Zhu M. Recent progress and advances in HGF/MET-targeted therapeutic agents for cancer treatment. *Biomedicines.* 2015;3:149–181.
26. Vosjan MJWD, Vercammen J, Kolkman JA, Stigter-van Walsum M, Revets H, van Dongen GAMS. Nanobodies targeting the hepatocyte growth factor: potential new drugs for molecular cancer therapy. *Mol Cancer Ther.* 2012;11:1017–1025.
27. Holland JP, Sheh Y, Lewis JS. Standardized methods for the production of high specific-activity zirconium-89. *Nucl Med Biol.* 2009;36:729–739.
28. Carlin S, Zhang H, Reese M, Ramos NN, Chen Q, Ricketts S-A. A comparison of the imaging characteristics and microregional distribution of 4 hypoxia PET tracers. *J Nucl Med.* 2014;55:515–521.
29. Lindmo T, Boven E, Cuttitta F, Fedorko J, Bunn PA Jr. Determination of the immunoreactive function of radiolabeled monoclonal antibodies by linear extrapolation to binding at infinite antigen excess. *J Immunol Methods.* 1984;72:77–89.
30. Toiyama Y, Miki C, Inoue Y, Okugawa Y, Tanaka K, Kusunoki M. Serum hepatocyte growth factor as a prognostic marker for stage II or III colorectal cancer patients. *Int J Cancer.* 2009;125:1657–1662.
31. To CT, Tsao MS. The roles of hepatocyte growth factor/scatter factor and met receptor in human cancers. *Oncol Rep.* 1998;5:1013–1024.